Microwave Noise in InP and SiGe HBTs: Modeling and Challenges

P. Sakalas[€,$], M. Schroter[€,§]

[€]Chair for Electron Device and Integrated Circuits, Technische Universität Dresden, 01062 Dresden, Germany,
[$]FRL, Semiconductor Physics Institute of Center of Physical Sciences and Technology, Vilnius-01108, Lithuania,
[§]ECE Dept., University of California, La Jolla, Gilman Drive, MS 0407 CA 92093-0407, USA.

***Abstract* -- DC, RF and noise characteristics of advanced InP/InGaAs DHBTs and Si/SiGe HBTs were measured and modeled in a broad frequency and temperature range. A systematic model for correlated noise in bipolar transistors and its implementation in HICUM/L0 v.1.31 and L2 v.2.31 is presented. The models were verified on SiGe HBTs up to 500 GHz with device simulation results from hydrodynamic and Boltzmann transport equation. HICUM with its implemented noise model also shows very good agreement with measured data in a broad frequency range. The verified model was used for noise analysis of advanced InP/InGaAs DHBTs and Si/SiGe HBTs. It was shown that shot noise correlation for high/speed InP/InGaAs DHBTs is not significant. Compared to Si/SiGe HBTs a higher noise at lower microwave frequencies was observed in InP/InGaAs DHBTs due to their high base recombination current. Nevertheless InP DHBTs show a good noise performance beyond 100 GHz and, due to better f_T BV_{CE0}, can compete with advanced Si/SiGe HBTs for LNA design**

Index-Terms: Compact model, f_T, f_{max}, HICUM, InP/InGaAs DHBT, Si/SiGe HBT, Noise parameters.

I. INTRODUCTION

Recent InP/InGaAs double-heterojunction bipolar transistor (DHBT) [1]-[7] and Si/SiGe HBT [8]-[13] process technology development has led to an increased interest in mm-band applications (e.g.,[14]-[20]). InP DHBTs are dominating in the high speed performance category, exhibiting record current gain cut-off frequencies (f_T) and maximum oscillation frequencies (f_{max}), e.g.: (f_T, f_{max}) = (0.36, 0.8) THz [7], (0.52, 1.1) THz [3], (0.43, 1.1) THz [2], (0.765, 0.24) THz [4] and (0.6, 0.3) THz [6]. InP DHBTs with a wide bandgap InP collector yield high f_T = 0.6 THz simultaneous with high breakdown voltages BV_{CE0} beyond 4 V, resulting in a record f_T BV_{CE0} of 2.53 THz V [6]. Due to those remarkable features InP DHBTs are used for analog sub-THz integrated circuits, such as microwave power amplifiers and LNAs [14]-[18],[20].

Recently, progress for SiGe HBT technology has led to (f_T, f_{max}) = (0.3, 0.5) THz [9],[10]. The potential of SiGe HBTs to reach even THz frequency of operation was predicted in [21]. Nevertheless due to the smaller Si bandgap, compared to InP, the f_T BV_{CE0} = 0.65 THz V sets on the limit to device scaling, likely to lead to a lower circuit performance[1]. An advantage of SiGe HBTs over InP DHBTs is a lower microwave noise, e.g.: NF_{min}= 0.5 dB at 1 GHz, 1.6 dB at 50 GHz [22],[23], 2.5 dB at 65 GHz, 4.2 dB at 170 GHz [24], 2.6 dB at 70 GHz [25], 1.9 dB at 67 GHz [26]. Therefore SiGe HBT technology is quite suitable for high speed LNAs [19],[26],[27].

Due to the higher base recombination current related shot noise, InP DHBTs do not seem to be among the best low noise devices, and there have not been many research papers dedicated to their high frequency (HF) noise investigation so far [28]-[32]. Older InP DHBT technologies demonstrated comparatively high noise figures: NF_{min}= 1.2 dB at 2 GHz, 3 dB at 20 GHz [28], 2 dB at 2 GHz, 6 dB at 18 GHz [29], 2.5 dB at 2 GHz, 3 dB at 18 GHz [30], 2 dB at 2 GHz, 2.8 dB at 26 GHz [31]. Most of those measurements were performed at frequencies not exceeding 26 GHz. Since the base current shot noise source is located at the input port, its impact on NF_{min} is more pronounced in the lower microwave band (i.e. below 40 to 50 GHz). However, due to their extremely high speed advanced InP/InGaAs DHBTs are expected to have fair noise performance at higher frequencies (i.e. beyond 50 GHz) and therefore could be used for HF LNA design. The associated gain (G_{ass}) of 8.4 dB with NF = 11.2 dB at 290-300 GHz [16] is comparable to state- of-the-art SiGe HBT LNA with NF = 13 dB at 220 GHz [27] and NF = 5.5 dB at 66 GHz [26] and even to LNAs with InP HEMT (known as a record low noise device) with G_{ass}=12 dB, NF =13 dB at 480 GHz [15]. Indeed, a compact model based noise parameter evaluation of an InP/InGaAs DHBT with a drawn emitter area of A_{E0} = 0.5 μm x 10 μm yields a competitive (to the state- of-the-art SiGe HBT [22]-[26]) noise performance: NF_{min}= 2.1 dB (50 GHz), 3 dB (100 GHz), 5.5 dB (300 GHz).

Efficient circuit design and optimization require compact models (CMs) accurately capturing the device characteristics over a wide bias, frequency, temperature and geometry range, [33, pp.486-496] including the HF noise behavior which is important for LNAs. Usually, HF noise measurements are complicated and require expensive equipment especially in HF: W, G (IEEE US) bands or special measures, such as imple-

1. As discussed in [21], BV_{CEO} in the ultimate limit will be limited by tunneling rather than impact ionization. Since BV_{CEO} is also often not the relevant breakdown voltage in, e.g., amplifier design, its value is of limited usefulness, especially when comparing technologies with very different current gain.

This work was financially supported by EU (DOTSEVEN), BMBF (RF2THz), DFG SCH695 and SFB912.

 978-1-4799-0671-0/13/$31.00

menting the entire noise parameter measurement system directly on-wafer to avoid losses [24],[25],[26]. The prediction of noise trend with a CM is the fastest and commonly used method in the design community. As a consequence, the accurate description of HF noise sources in CMs has become of importance. Since both InP and SiGe HBTs technology are being used for mm-wave LNA design this work focuses on their noise modeling and related problems.

II. DUT AND EXPERIMENTAL

We have investigated InP/InGaAs DHBTs with a CBEBC contact configuration and emitter area of $A_{E0} = 0.7\ \mu m$ x $8\ \mu m$ featuring $(f_T, f_{max}) = (240, 380)$ GHz [1]; InP/InGaAs DHBTs from Teledyne Scientific Company with CBEBC configuration with $A_{E0} = 0.5\ \mu m$ x $10\ \mu m$ and $(f_T, f_{max}) = (330, 370)$ GHz [2],[34]; Si/SiGeC HBTs in CBEBC configuration with $A_{E0} = 0.13\ \mu m$ x $10\ \mu m$ and $(f_T, f_{max}) = (260, 350)$ GHz [11] as well as with $A_{E0} = 0.12\ \mu m$ x $10\ \mu m$ and $(f_T, f_{max}) = (310, 400)$ GHz [12]; Si/SiGeC CEB HBTs with $A_{E0} = 8$ x ($0.12\ \mu m$ x $0.96\ \mu m$), $(f_T, f_{max}) = (300, 500)$ GHz [9],[10].

On-wafer DC and AC (frequency range 0.1-110 GHz) standard characteristics were measured with a PNA 8361C and HP4142. Noise parameters in source-load matching conditions were measured in the 1 to 8 and 8 to 50 GHz frequency range with a Maury Microwave automated tuner system ATS and impedance tuners MT982 and MT984A01. The de-embedding of the pad parasitics was performed with a 2-step method by using "open" and "short" dummies, whereas for the noise parameter de-embedding the correlation matrix technique was employed.

III. NOISE MODELING

For noise calculations the transistor can be treated as a linear ergodic system, described by a two-port. The noise evaluation of such a system is performed by the calculation of the noise factor F or noise figure NF [35]. For the NF simulation the output noise power spectral density of the system (Y) is determined (cf. Fig. 1 (c)), which is determined by the number of intrinsic noise sources X_1, X_2 in the two port in Fig. 1 (a).

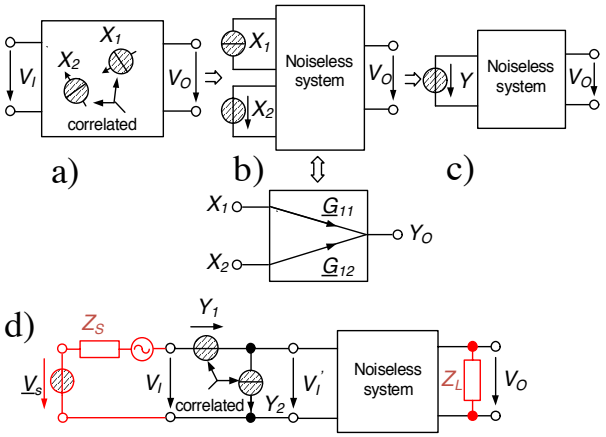

Fig. 1. Systematic implementation of correlated internal noise sources for NF calculation, following [22]. (a) noisy two-port, (b) noiseless system with the noise sources, transferred to the input, (c) noiseless two-port with output noise source Y, (d) noiseless two-port system with correlated extrinsic noise sources embedded in the source generator and load (to establish output short-circuit) system for NF calculation. V_1, V_2 are input and output bias, Y_o is the output noise source, $\underline{G}_{11}$, $\underline{G}_{22}$ are transfer functions, Z_S is the noisy source generator impedance, V_1' is the internal bias.

In HBTs the base and collector current shot noise can be treated as sources X_1, X_2 in the system of Fig. 1. X_1, X_2 can be correlated. Due to the different physical origin of the base and collector currents, collector current shot noise is correlated to the dynamic base current shot noise only (e.g. p. 492 [33]).

The noise power spectral density (PSD) S_Y at the system output in general is calculated following [35],[36]:

$$\boldsymbol{S_Y}(j\omega) = \mathbf{G}(j\omega) \cdot \mathbf{S_{XX}}(j\omega) \cdot \mathbf{G}^{\dagger}(j\omega)\,, \tag{1}$$

where $\mathbf{G}^{\dagger}(j\omega)$ and $\mathbf{S_{XX}}(j\omega)$ are the adjunct transfer and input PSD matrices. Solution of (1) for the two-port yields [22]

$$\boldsymbol{S_Y} = \sum_{j=1}^{2}\sum_{i=1}^{2} \underline{\boldsymbol{G}}_{1i}\underline{\boldsymbol{G}}^{*}_{1j}\boldsymbol{S_{Xij}}\,. \tag{2}$$

Further simplification of (2) for uncorrelated internal noise sources [22] results to

$$\boldsymbol{S_Y} = \sum_{i=1}^{2} \left|\underline{\boldsymbol{G}}_{1i}\right|^2 \boldsymbol{S_{Xii}}\,. \tag{3}$$

The latter neglects correlation. Nevertheless it is used in commercial circuit simulators. The noise factor F is calculated according to (2) or (3):

$$\boldsymbol{F} = \frac{\boldsymbol{S_Y}}{\boldsymbol{S_{im}}}\,, \tag{4}$$

Since noise correlation is very important for HBTs [23] the problem to force the circuit simulator to account for it was solved and realized following the general approach described in [22]. The Verilog-A code of HICUM/L2 with adjunct network as shown in Fig. 2 was used.

The noise PSD of the collector and base current in HICUM/L2 are calculated based on the an der Ziel noise model [36] after modification from the original injection (T-type) model to the more practically useful π model:

$$\boldsymbol{S_{inb}} = 2\boldsymbol{q}\boldsymbol{I_B}[1 + 2\alpha_{\boldsymbol{qf}}\boldsymbol{B_f}(\omega\tau_{\boldsymbol{Bf}})^2]\,, \tag{5}$$

$$\boldsymbol{S_{inc}} = 2\boldsymbol{q}\boldsymbol{I_C}\,, \tag{6}$$

where S_{inb} is the PSD of the base current shot noise, S_{inc} is the collector current shot noise PSD, I_B is the DC base current, B_f is the DC current gain of the internal transistor, τ_{Bf} is the forward base transit time of the internal transistor, and α_{qf} is the ratio (≤ 1) of the minority charge related nonquasistatic (NQS) delay time to τ_{Bf}.

A detailed derivation of the bipolar transistor PSDs showed that correlation is closely related to the NQS effect in the collector current since its frequency dependence is determined by

the NQS expression and associated time constant of the transconductance [33, p. 493]. Thus, the noise correlation related PSD is described by [22]:

$$\underline{S}_{inbinc} = j\omega\tau_{Bf}\alpha_{it}2qI_C\,, \tag{7}$$

with α_{it} as the ratio (≤ 1) of the transfer current related NQS delay time to τ_{Bf}. The derivation of the NQS effect description and (7), [33, p. 493] does not lead to an exponential delay term, such as

$$S_{inb} = 2qI_B[1+\left|1-e^{-j\omega\tau}\right|^2 I_C]\,, \tag{8}$$

$$\underline{S}_{inbinc} = 2qI_C(e^{j\omega\tau}-1)\,, \tag{9}$$

which is often used for noise modeling [37],[38]. Above expressions, with τ as a noise delay time, are only an approximation of (5) and (7). Note that exponential terms such as those in (8) and (9) cannot be used in time domain analysis of NQS effects.

Noise parameters were simulated by using HICUM with implemented shot noise correlation [22]. For the InP/InGaAs DHBTs HICUM/L0 and for Si/SiGeC HBTs HICUM/L2 (cf. Fig. 2) were employed. The implemented noise correlation model had already been verified for Si/SiGe HBTs [22],[23] but not for InP/InGaAs DHBTs, where nonequilibrium transport is more pronounced.

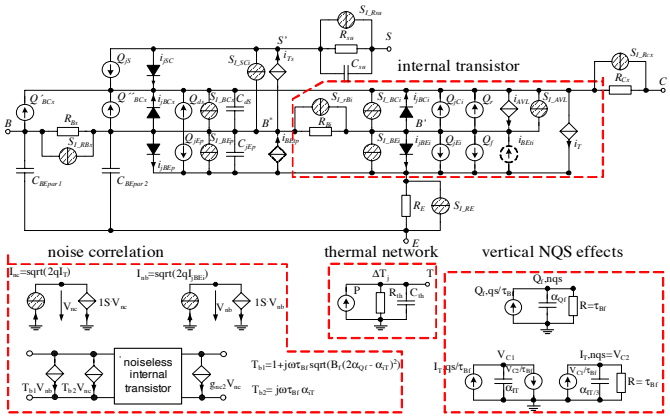

Fig. 2. Equivalent circuit (EC) of the compact model HICUM/L2 with correlated noise, NQS and thermal subcircuits.

The EC of HICUM/L0 is not given here due to the lack of space, but can be found in [33]. Its latest version 1.3 contains the same noise, thermal and NQS subcircuits as L2.

IV. RESULTS AND DISCUSSION

Typical band diagrams of an InP/InGaAs DHBT and Si/SiGeC HBT are given in Fig. 3. The high electron mobility in the InGaAs base allows a thicker layer, which is usually heavily doped to reduce the base resistance. Nevertheless due to the low hole mobility (~50 cm^2/Vs.) the base resistance remains still significant. For improving the speed, the InP base can have a graded base doping which creates a built-in field for accelerating the electrons. Different from SiGe HBTs to prevent charge pile-up due to BC barrier and non-equilibrium (NE) transport in the collector, a delta-doping or superlattice layer are usually grown in the collector [2],[3].

Since the electron mobility in SiGe is lower compared to InGaAs a graded Ge profile has always been used to accelerate minority carriers across the base [39, p.391]. The associated band diagram is shown in Fig. 3 (b). For preventing B outdiffusion in the base carbon doping is used, leading to a Si/SiGeC HBT. Among the investigated InP/InGaAs DHBTs both were used, one with a delta-doped layer [1] and another with superlattice layer [2],(cf. Fig. 3 (a)).

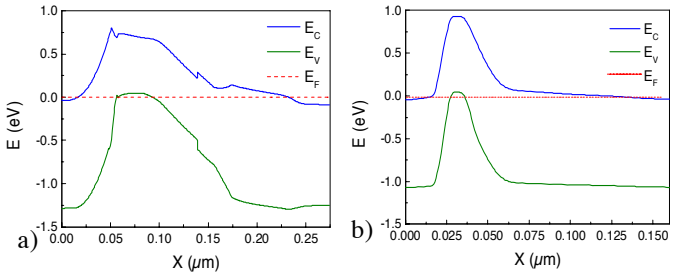

Fig. 3. Typical equilibrium band diagrams of (a) InP/InGaAs DHBT and (b) Si/SiGe HBT.

The noise model was verified on Si/SiGeC HBTs with $A_{E0} = 0.13\ \mu$m x 10 μm, $(f_T, f_{max}) = (260, 350)$ GHz [11] as shown in Fig. 4. HF noise parameters were measured up to 50 GHz and simulated with HD model and HICUM.

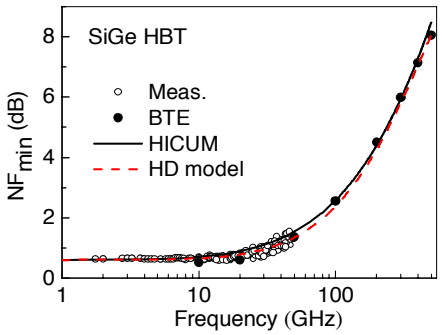

Fig. 4. NF_{min} vs. frequency for SiGe HBT [11] at $J_C = 10$ mA/μm^2, $V_{CE} = 1.2$ V [22],[23].

In order to extend the verification of both models beyond 50 GHz to the mm-wave and sub-THz range, the Boltzmann transport equation was solved as shown in Fig. 4. Note that the noise model implemented in HICUM so far had not been verified for III-V based HBTs and more advanced SiGe HBT technologies.

A. InP/InGaAs DHBT: DC, RF and noise characteristics.

Measured and simulated forward output characteristics of InP/InGaAs DHBT with a base current drive are given in Fig. 5. HICUM/L0 v.1.31 yields very good agreement. Devices can operate up to $V_{CE} = 4.5$ V, featuring $B_f = 90$ [1]. At higher V_{CE} significant self-heating occurs, reducing the collector current for I_B driven output characteristic and vice versa if V_{BE} is fixed. The wafer substrates used in III-V devices typically have a low thermal conductivity so that heat dissipation is a problem, possibly leading to device thermal breakdown.

The forward Gummel plot of with different emitter widths and areas is shown in Fig. 6. The visibly high recombination current component in the base current results in a relatively

low DC current gain (~90) compared to SiGe HBTs (i.e. up to several 1000, cf. Fig. 12).

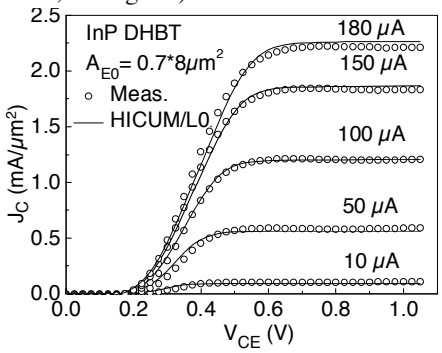

Fig. 5. Collector current density $J_C(V_{CE})$ versus I_B. Technology details can be found in [1].

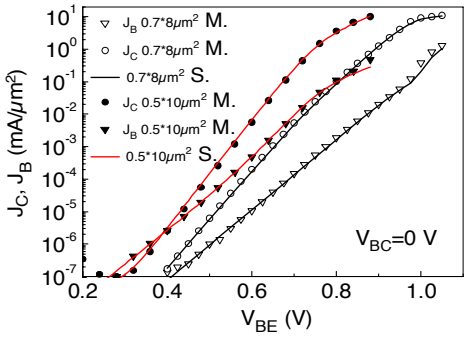

Fig. 6. J_C and J_B vs. V_{BE} at V_{BC} = 0 V of an InP DHBT with A_{E0} = 0.7 μm x 8 μm (open symbols) and A_{E0} = 0.5 μm x 10 μm (solid symbols). Lines represent HICUM./L0.

Measured and modeled f_T and f_{max} at V_{BC} = 0 V are presented in Fig. 7. InP/InGaAs DHBTs with A_{E0} = 0.5 μm x 10 μm and A_{E0} = 0.7 μm x 8 μm exhibit f_T/f_{max} = 300/280 GHz and f_T/f_{max} = 220/270 GHz respectively, which are fairly well accounted by HICUM/L0. NE transport is slightly evident: a sharp increase of f_{max} with current density in the range of J_C from 0.07 to 2 mA/ m^2 is present, which can not be captured by the model. For example for GaAs/InGaP HBTs NE effect is much more pronounced, p.97 [41, p. 97], resulting to a very sharp f_T and f_{max} increase [42],[43].

The high recombination current impacts also the HF noise performance as it increases the shot noise and related noise figure especially at lower microwave frequencies. Noise modeling and the behavior of NF_{min} in Fig. 8 and Fig. 9 do not show any noise reduction related to Coulomb blocking as was observed in GaAs based HBTs [42],[43].

The bias dependence of NF_{min} at 10 GHz shows a slight maximum at J_C = 0.007 mA/μm², which is related to the shot noise source equalization to the thermal noise in R_B. The bias dependence of highly doped ($5 \cdot 10^{19}$cm^{-3}) base resistance is smaller in InP DHBT, compared to Si/SiGe HBT, and therefore this maximum is less pronounced, compared to SiGe HBTs. Simulations show that without the thermal noise of R_B, this maximum disappears, Fig. 9, dashed-dotted line. The noise data does not show any significant shot noise correlation at least up to 50 GHz frequency. An impact of shot noise correlation starts beyond about 100 GHz as can be seen in Fig. 10 (dashed and solid lines). Noise analysis reveals that noise trend could be improved by base resistance, recombination current and emitter width (b_{E0}) reduction in InP/InGaAs DHBTs which is a challenge. b_{E0} reduction draw back is higher R_B which can be compensated by higher base doping, which results in higher base recombination current and thus worse noise.

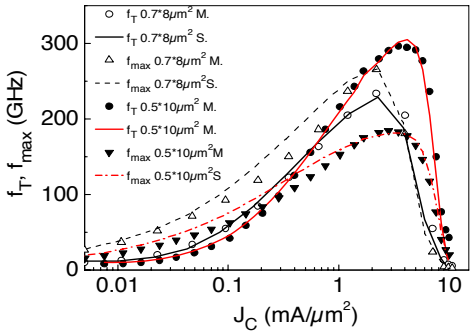

Fig. 7. f_T and f_{max} vs. J_C at V_{BC} = 0 V of InP DHBTs with A_{E0} = 0.7 μm x 8 μm (open symbols) and A_{E0} = 0.5 μm x 10 μm (solid symbols). HICUM are lines.

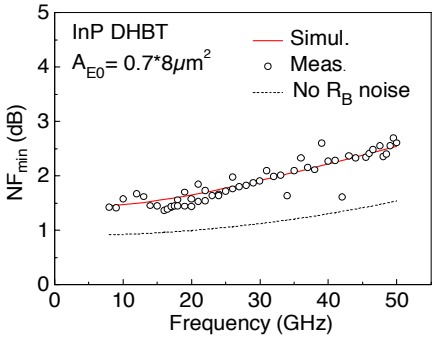

Fig. 8. NF_{min} vers. frequency at J_C = 0.68 mA/μm², V_{CE} = 1 V. An external R_{BX} and internal R_{Bi} base resistances (cf. Fig. 2) in HICUM/L0 are merged to R_B.

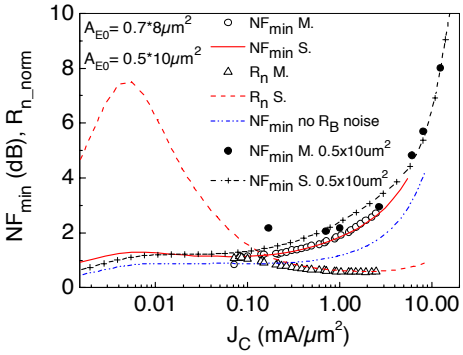

Fig. 9. NF_{min} and normalized to 50 Ω noise resistance R_{n_norm} vs. current density at 10 GHz and V_{CE} = 1 V for InP DHBT with A_{E0} = 0.7 μm x 8 μm and NF_{min} at 5 GHz, V_{CE} = 1.5 V for InP DHBT with A_{E0}= 0.5 μm x 10 μm.

Compared to advanced Si/SiGeC HBTs (solid symbols in Fig. 10), the 0.5 μm emitter width InP/InGaAs DHBT has a higher noise up to ~ 60 GHz. However, beyond about 60 GHz, the NF_{min} of InP DHBTs becomes as good as that of SiGe based HBTs (cf. Fig. 10). Shot noise correlation for this InP/InGaAs technology transistor is negligible (cf. Fig. 10, solid line and dashed-dotted curves). The noise factor ($NF_{50\Omega}$ in 50 Ω environment, no source impedance matching) at cryogenic environment versus frequency is presented in Fig. 11. InP/InGaAs DHBTs can operate even at T=10 K. The high

base doping ($5{\cdot}10^{19}$cm^{-3}) prevents the carriers from freezout, yielding 22 dB of associated gain (G_{ASS}) and $f_T = 450$ GHz. The lower G_{ASS} at $T = 77$ K is related to the bias point selection. The observed weak temperature and frequency dependence of $NF_{50\Omega}$ can be explained by the domination of the base current shot noise component.

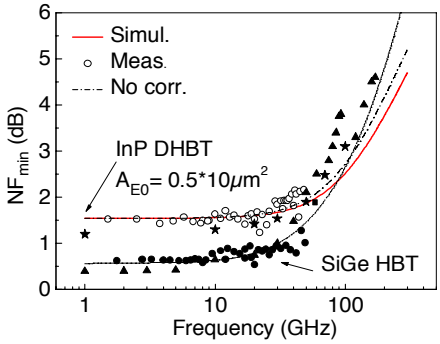

Fig. 10. Measured (open symbols) and simulated NF_{min} vs. frequency at $J_C = 0.497$ mA/μm^2, V_{CE}=1.5 V. Solid circles represent results from advanced 0.13 μm Si/SiGeC HBT [22], dotted line is data from hydrodynamic model [22], stars are data from 0.13 μm SiGe HBT [11], triangles are NF_{min} of 0.13 μm Si/SiGeC HBT [24].

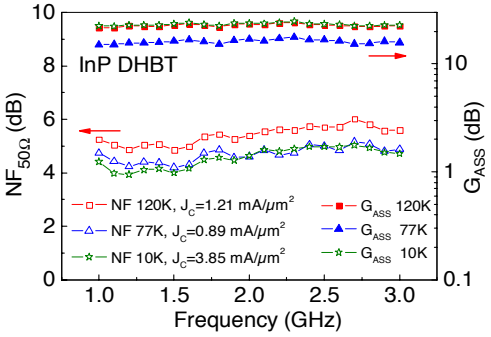

Fig. 11. $NF_{50\Omega}$ and associated gain vs. frequency at $V_{CE} = 1$ V for different temperatures for InP DHBT with A_{E0}= 0.7 μm x 4 μm.

B. Si/SiGe HBT: DC and RF and noise characteristics.

The forward Gummel plot of a Si/SiGeC HBT with $A_{E0} = 8$ x (0.12 μm x 0.96 μm) is shown in Fig. 12. HICUM/L2 v.2.31 simulations are in a perfect agreement with measured data (cf. Fig. 12, Fig. 13, Fig. 14). The very thin base layer with a doping gradient enables low recombination current and high speed (Fig. 13). Note that the SiGe technology used in this work (not this transistor) [9],[10] yields a record for Si/SiGeC HBTs $f_{max} = 500$ GHz. High speed in Si/SiGeC HBTs is achieved by reducing the base width and increased collector doping. The peak value of f_T in Si/SiGeC HBT already lies at values of J_C higher, compared to InP based HBTs: J_C >10 mA/m^2. The high collector doping insets collector breakdown to $BV_{CE0} = 1.6$ V. Further speed improvement, as predicted in [21], requires even stronger vertical downscaling, with a drawback of increasing tunneling current density and decreasing BV_{CE0}. The very low noise of Si/SiGeC HBTs with $A_{E0} = 8$ x(0.12 μm x 0.96 μm) is well captured by the implemented noise model (cf. Fig. 14). Simulations show that correlated noise starts to be significant beyond around 50 GHz. The proposed noise model was also successfully verified for a different technology [23].

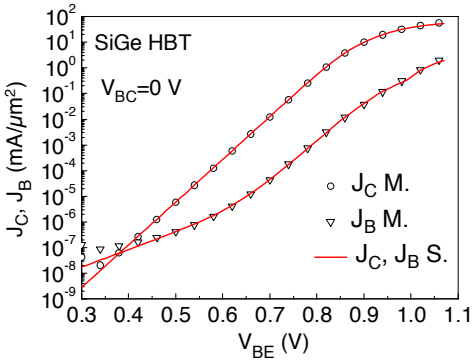

Fig. 12. J_C and J_B vs. V_{BE} at $V_{BC} = 0$ V of Si/SiGeC HBT with $A_{E0} = 8$ x(0.12 μm x 0.96 μm) (symbols) and HICUM/L2 (lines).

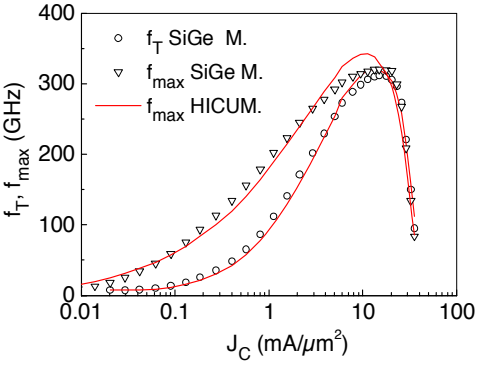

Fig. 13. Measured (symbols) and HICUM/L2 (lines) f_T and f_{max} vs. J_C, $V_{BC} = 0$ V for the Si/SiGeC HBT with $A_{E0} = 8$ x(0.12 μm x 0.96 μm).

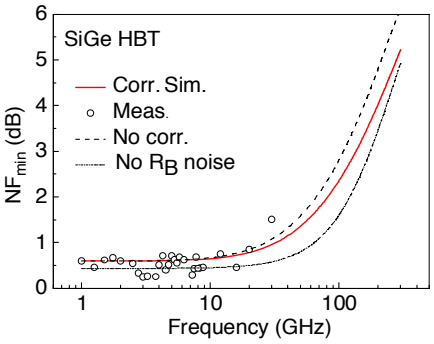

Fig. 14. Measured (symbols) and HICUM/L2 (lines) NF_{min} vs. frequency of Si/SiGeC HBT with $A_{E0} = 8$ x(0.12 μm x 0.96μm) at $J_C = 6.78$ mA/μm^2, $V_{CE} = 1.2$ V..

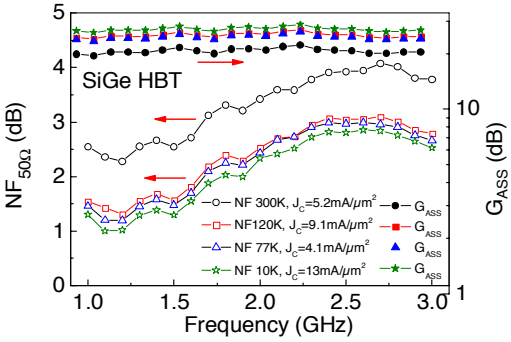

Fig. 15. $NF_{50\Omega}$ and G_{ASS} vs. frequency at $V_{CE} = 1.0$ V, for different temperatures for Si/SiGeC HBT with A_{E0}= 8 x(0.12 μm x 0.96 μm).

Si/SiGeC HBTs can operate at cryogenic temperatures without a significant carrier freezout [39, p.497],[40]. Compared to

T = 300 K, the noise improvement of Si/SiGeC HBT at 10 K is significant. This confirms that for Si/SiGeC HBT at lower microwave frequencies $NF_{50\Omega}$ is mainly shaped by the thermal noise in resistive components. The value of $NF_{50\Omega}$ = 1 dB at 1 GHz corresponds to NF_{min} ~ 0.1 dB in matched conditions.

V. CONCLUSIONS

A systematic noise correlated model implementation to the compact models HICUM/L0 and L2 are presented. Models were verified on both hydrodynamic model and Boltzmann transport equation, for Si/SiGeC HBTs up to 500 GHz. InP/InGaAs DHBTs with A_{E0} = 0.5 μm x 10 μm, A_{E0} = 0.7 μm x 8 μm and a high speed Si/SiGeC HBT with A_{E0} = 8 x(0.12 μm x 0.96 μm) were investigated. It was shown that shot noise correlation for InP/InGaAs HBTs is not significant at least up to 100 GHz and that InP/InGaAs DHBTs due to the high base recombination current, exhibit higher noise at lower microwave frequencies as compared to Si/SiGeC HBTs. However InP DHBTs show a good noise performance beyond 100 GHz and due to better $f_T BV_{CE0}$ can compete with advanced Si/SiGeC HBTs for LNA design at G band.

High speed Si/SiGeC HBTs exhibit very low NF_{min} in a wide frequency band. The impact of correlated noise on NF_{min} has been observed at frequencies beyond 100 GHz. It was shown that both InP and SiGe technology transistors can operate at cryogenic temperatures, resulting in f_T, f_{max} = 450, 400 GHz for InP/InGaAs DHBTs with A_{E0}= 0.7 μm x 8 μm and f_T, f_{max} = 450, 700 GHz for Si/SiGeC HBTs with A_{E0}= 8 x(0.12 μm x 0.96 μm) at T=10 K.

Noise behavior in InP/InGaAs DHBTs can be improved by vertical scaling and reduction of base resistance, recombination current as well as further reduction of emitter width. Low noise/high speed improvement in Si/SiGe HBTs requires stronger vertical downscaling, resulting in increased J_C tunneling current and decrease of BV_{CE0}.

ACKNOWLEDGEMENT

We are thankful to B. Heinemann, B. Tillak from IHP (Frankfurt-Oder, Germany), U. Nowotny, R. Driad, M. Schlechtweg from Fraunhofer IAF (Freiburg, Germany), M. Urteaga (Teledyne Scientific) and P. Chevalier from ST Microelectronics for providing wafers. We are in debt to A. Mukherjee for support with Verilog-A, A. Pawlak and T. Nardmann (all from CEDIC TU Dresden) for the help with HICUM parameter extraction.

REFERENCES

[1] R. Driad *et al.*, *IPRM*, pp.10-15, 2009.

[2] M. Urteaga *et al.*, 23rd Int. Conf. *IPRM*, 2011.

[3] M. Urteaga *et al.*, 69th *Annual Device Research Conference*, pp.281-282, 2011.

[4] W. Snodgrass, W. Hafez, N. Harff, M. Feng, *IEDM'06*, 2006.

[5] M. Feng, W. Snodgrass, 19th Int. Conf. *IPRM*, pp.399-402, 2007.

[6] H. G. Liu *et al.*, *IEDM 2007*, pp.667-670, 2007.

[7] E. Lobisser *et al.*, *IEEE IPRM*, pp.16-19, 2009.

[8] H. Rücker *et al.IEEE Journ. of Solid-State Circuits*, Vol.45, No.9, pp.1678-1686, 2010.

[9] B. Heinemann *et al.*, Proc. *IEDM'10*, pp.688-691, 2010.

[10] H. Rücker, B. Heinemann, A. Fox, *SiRF'12*, pp.133-136, 2012.

[11] G. Avenier *et al.*, *IEEE Journal of Solid-State Circuits*, Vol.44, No.9 pp.2312-2321, 2009.

[12] P. Chevalier *et al.*, Proc. *IEEE BCTM 1.4*, pp. 1-4, 2009.

[13] S. Decoutre *et al.*, Proc. *IEEE BCTM 1.3*, pp. 9-16, 2008.

[14] M. Urteaga *et al.*, Proc. *IEEE, MTT IMS'10,* 2010.

[15] W. R. Deal, Proc. *IEEE MTT IMS'10,* pp. 1122-1125, 2010.

[16] J. Hacker *et al.*, Proc. *IEEE MTT IMS'10*, pp. 1126-1129, 2010.

[17] J. Hacker *et al.*, Proc. *IEEE MTT IMS'08*, pp. 403-406, 2008.

[18] L. A. Samoska, *IEEE Trans. on Terahertz Science and Technology*, Vol. 1, No. 1 pp.9-24, 2011.

[19] R. Reuter, Y. Yin, Proc. *BCTM 7.2*, 2006.

[20] T. Reed *et al.*, *IEEE.MTT IMS'12*, 2012.

[21] M. Schroter *et al.*, *IEEE Trans. on Electron Dev.*, Vol. 58, No. 11, pp. 3687-3696, 2011.

[22] J. Herricht *et al.*, *IEEE Trans. on Microw. Theory Tech.,* Vol.60, No.11, pp. 3403-3412, 2012.

[23] P. Sakalas *et al.*, Proc. *IEEE BCTM'10 9.5*, pp. 169-172, 2010.

[24] K. H. Yau *et al.*, *IEEE Trans.on Microw. Theory Tech.,* Vol.59, No.8, pp. 1983-2000, 2011.

[25] Y. Tagro, *et al. BCTM 6.1* pp. 83–86, 2009.

[26] T. Quemerais *et al.*, *IEEE Radio Frequency Integrated Circuits Symposium*, pp. 351-354, 2012.

[27] E. Öjefors, B. Heinemann, U. Pfeiffer, *IEEE Trans on Microw. Theory Tech.,* Vol.60, No.5 pp. 1397-1404, 2012.

[28] Y. Z. Xiong *et al., IEEE Trans. Electron Devices*, Vol. 49, No. 7, pp. 1308-1311, 2002.

[29] Y.-K. Chen *et al.*, *IEEE Electron Device Letters*, Vol.10, No.10, pp. 470-472, 1989.

[30] V. Danelon *et al.*, *IEEE Microwave Guided Wave Letters*, Vol.9, No.5, pp. 195-197, 1999.

[31] A. Huber *et al.*, Proc. of 20th *Workshop on Comp. Semic. Dev. and Integ. Circ.* (*WOCSDIC*), May 19-22, Lithuania, pp. 83-84, 1996.

[32] S. S. H. Hsu, D. Pavlidis, M. Ida, T. Enoki, *IEEE GaAs Digest*, pp. 188-191, 2001.

[33] M. Schroter, A. Chakravorty, Compact Hierarchical Bipolar Transistor Modeling with HICUM, World Scient. Pub. Company, ISBN-10: 981427321X, ISBN-13: 978-9814273213, p. 752.

[34] M. Urteaga *et al.*, *IPRM'08*, 20th Int. Conf., pp. 1-5, 2008.

[35] H. A. Haus *et al.*, Proc. of the *IRE*, pp. 69-74, 1960.

[36] A. van der Ziel, G. Bosman, *IEEE Trans. Electron Devices*, Vol.31, No.9, pp. 1280-1283, 1984.

[37] M. Rudolph *et al., IEEE Trans. Microw. Theory Tech.,* Vol.56, No.1, pp. 7-14, 2008.

[38] K. Xia *et al.*, *IEEE Trans. Electron Devices*, Vol.53, No.3, pp. 515-522, 2006.

[39] J. D. Cressler (ed.), The silicon heterostructure handbook, CRC Press NY, 2005.

[40] H.Geissler, A.Rumiantsev, S.Schott, P.Sakalas, M.Schröter, Proc. 68th *ARTFG Microw. Meas.Conf.* pp.67-73, 2006.

[41] B. Jalali, S. J. Pearton, InP HBTs: Growth, Processing and Applications, Artech House, ISBN 0-89006-724-4, p. 421.

[42] A. Shimukovitch *et al., Phys. Status Solidi RRL* 4, No. 11, pp. 335–337, 2010.

[43] P. Sakalas *et al.*, Proc. 18th, *ICNF'05*, ed. T. Gonzalez, J. Mateos, D. Pardo, 2005 American Institute of Physics ISBN 0-7354-0267-1/05/$22.50, pp. 303-306, 2005.